Experimental Verification of Control Strategies for Satellite Magnetic-Based Attitude Control System Under a Three-Axis Helmholtz Cage Environment

Thanayuth Panyalert*†, Shariff Manuthasna†, Jormpon Chaisakulsurin†, Tanawish Masri†,
Kritsada Palee†, Pakawat Prasit†, Peerapong Torteeka†, Pasu Poonpakdee*, and Poom Konghuayrob*‡‡
*School of Engineering, Department of Robotics and Artificial Intelligence,
King Mongkut's Institute of Technology Ladkrabang,
No.1, Chalong-Krung, 1-Alley, Ladkrabang, Bangkok 10520, Thailand.
†Thai Space Consortium Project, and Center of Observatory Operation and Engineering,
National Astronomical Research Institute of Thailand (Public Organization)
No.260, Don-Kaew, Mae-Rim, Chiang-Mai 50180, Thailand.
‡‡Corresponding author E-mail: poom.ko@kmitl.ac.th

***Abstract*—During satellite mission planning and operation, the main function of the satellite's attitude determination and control subsystem (ADCS) is to gather information about the satellite's orientation relative to the inertial reference frame. Additionally, this subsystem generates control actions that produce the required torques for adjusting the satellite's orientation, particularly in the context of the Low-Earth Orbit (LEO) regime. This paper focuses on the satellite three-axis attitude control problem for a de-tumbling mode of spacecraft using only magnetorquers as actuators under the presence of noise and investigates their performance through Hardware-in-the-Loop simulation (HiLs) tests, which consisted of a relative Earth's magnetic field generator along with the SGP-4-based satellite orbital propagator high-level control software. The design, development, and verification of proposed satellite attitude control system (ACS) strategies are presented. In detail, as an example of experimentation, the classical B-dot control algorithm is used for the de-tumbling mode to stabilize and reduce the angular rate, along with the pointing algorithm for orienting the satellite to the desired attitude. Then, a cascade Proportional–Integral–Derivative (PID) is implemented to generate enough torque through the three-axis magnetorquers on the frictionless air-bearing platform to verify the performance of the controller using an onboard computer. Finally, the effectiveness of the co-simulation tested as the primary experiment was confirmed through the integrated simulation process.**

***Index Terms*—Satellite Attitude Control System, Three-Axis Magnetorquers, Hardware-in-the-Loop simulation, and Control Strategies.**

I. Introduction

The attitude determination and control subsystem (ADCS) is crucial for ensuring satellite orientation stability and precision when pointing various payloads at specific targets. It comprises two subsystems: Attitude Determination (ADS), which employs sensors to determine the satellite's attitude or angular rates, and Attitude Control System (ACS), which utilizes actuators, control algorithms, and controllers to maneuver the satellite to the desired orientation [1]. The magnetoquer is a form of ACS actuator that generates a magnetic field in order to interact with the Earth's magnetic field (EMF), which is efficient and reliable, especially in low Earth orbit [2]. To prepare the satellite for the nominal mission, the ADCS needs to ensure controllability of its attitude by reducing its initial angular rate and stabilizing the spinning with high angular rates in the de-tumbling phase of the satellite's attitude after its launch to orbit [3]. For this reason, Hardware-in-the-Loop simulation (HiLs) is an intriguing approach used to test and validate software algorithms for guidance, navigation, and control in a ground-based environment.

The HiLs setup consists of several components. The Helmholtz cage, a crucial device, is capable of simulating the EMF vector experienced by the satellite during its orbital motion. The magnetometer is integrated into the simulation loop to provide feedback on the magnetic field. Additionally, the setup includes an air-bearing platform that facilitates quasi-frictionless rotational motion, essential for simulating the attitude dynamics of the satellite under the control of the magnetic-based ACS [4], [5]. Verifying the satellite process through the HiLs can help save resources, time, and costs. The information given by HiLs assisted the designer in reviewing failure causes and adjusting the control algorithm [6].

In recent years, research on satellite ACS has been fascinating [7]. Linear strategies controllers, such as the PID controller, are utilized; this method is extensively used in ACS and has a simple structure and good stability [8]. Several control techniques have also been approved. However, ground testing, such as HiLs, is still required to continuously improve the performance of the ACS system [9]. Thus, verification and validation of the control strategy through ground-based testing through the HiLs is critical to ensuring that the developed ACS can provide stabilization after deployment. This work primarily focuses on validating the effectiveness of the control algorithm tested through HiLs using a three-axis magnetorquer to de-tumble the satellite model during the de-tumbling phase scenario and verifying the cascade PID controller's performance using an onboard computer.

This paper is organized as follows: The three-axis Helmholtz cage, which is the main equipment of the HiLs architecture, is introduced in Section II. Section III presents the satellite magnetic-based attitude control system methodology, including the attitude dynamics and kinematics, satellite attitude model and control system, magnetorquer model, and

979-8-3503-0219-6/23/$31.00 ©2023 IEEE

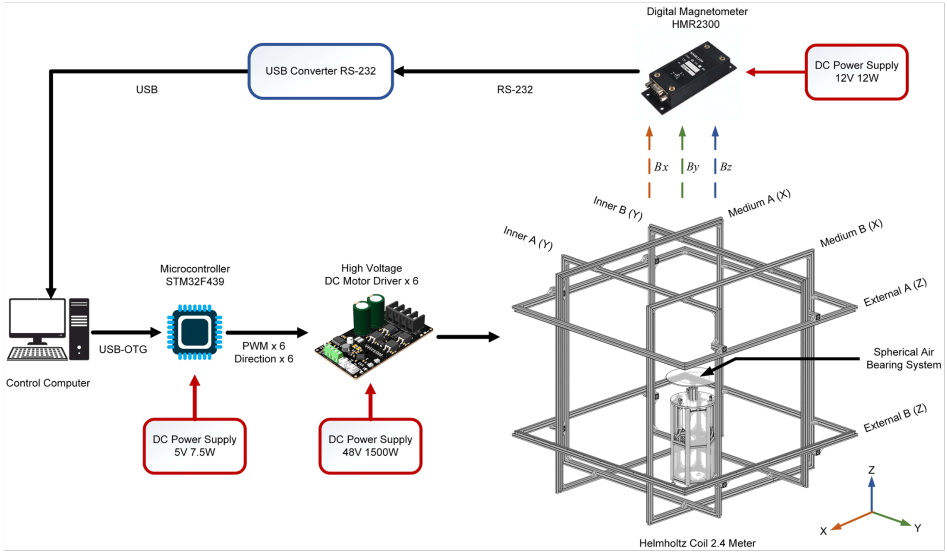

Fig. 1. A system architecture of the proposed HiLs testbed.

HiLs platform. Section IV presents numerical simulations to illustrate the control strategy's effectiveness. Finally, in Section V, the conclusions and future works are presented.

II. Hardware-in-the-Loop System Architecture

A. Three-Axis Helmholtz Cage

The primary equipment used for generating the EMF based on Biot-Savart's law, specifically for ACS validation, is the three-axis Helmholtz cage. This cage consists of a pair of co-axial and parallel square coils. The proposed three-axis square Helmholtz coil has the capability to uniformly generate an EMF of 1±0.5 G within a cubic-like area of 0.5 meters from the center. Furthermore, the boundary parameters of the EMF can also be utilized to estimate the integral wind-up in the PID controller and ensure that the control signal remains within the limits of the actuator, which is restricted by the wire size. In accordance with the mission requirements, the design of the Helmholtz coil should be simple to construct, wind, and bend at the corners. Referring to the system architecture depicted in Figure 1, a DC power supply model, specifically the TDK-Lambda with 48V and 1500W, was employed as the low-level control software. This power supply controlled the voltage sources in coordination with six high-voltage Cytron DC motor drives. Each motor drive was independently responsible for controlling the direction and intensity of the magnetic field for its respective Helmholtz coil using a PWM signal derived from a 32-bit STM32F439 microcontroller running at a frequency of 180 MHz. The microcontroller itself was powered by a 5V low-voltage power supply. The high-level control software, developed using C# programming, is responsible for generating the EMF command. It achieves this by utilizing the SGP4-based satellite orbit propagator. Additionally, the software provides closed-loop feedback on the EMF characteristics using the Honeywell magneto sensor, which is powered by a 12V low-voltage power supply. The detailed technical specifications of the HiLs have been presented in Table 1.

Using affordable components, the square-shaped Helmholtz coils, measuring 2.4 meters, have been developed

TABLE I
The HiLs testbed sub-system specification.

Sub-systems	Model	Parameters
DC Motor Drive	Cytron MD25HV (6 Pcs.)	Input Voltage: 7-58 V Max output current: 25A Output PWM Freq.: 16 kHz
Micro-controller	NUCLEO-F439ZI (1 Pc.)	Model type: ARM Cortex-M4 32-bit Clock Freq.: 180 MHz Flash memory: 2 Mbyte I/O Ports: 168 I/O
Power supply	TDK-Lambda CUS1500M-48/RF (1 Pc.)	Output voltage: 48V Output Current: 32A Output Power: 1.536kW
	CUI Inc. SMM12-12 (1 Pc.)	Output voltage: 12V Output Current: 1A Output Power: 12W
	Delta DRC-5V 10W1AZ (1 Pc.)	Output voltage: 5V Output Current: 1.5A Output Power: 7.5W
Magnetic field sensor	Honeywell HMR2300 (1 Pc.)	Range: ±2 G Three Axis Digital Output Data Interface: RS232 Sample rate: 10-154 Sam/S

to generate a uniform EMF during three-axis functional testing on the ground. The HiLs demonstrates its capability to generate an EMF within a range of 1±0.5 G with uniformity across a one-meter cubic-like area centered within the cage. This feature makes it suitable for conducting ground-based HiLs for attitude control of micro-satellites in de-tumbling mode, utilizing the B-Dot control algorithm.

III. Satellite Magnetic-Based Attitude Control System Methodology

A. Magnetic Attitude Dynamics and Kinematics

The magnetic attitude dynamics are modeled by considering the rotation of the spacecraft when using magnetic actuation. The spacecraft is described as a rigid body with

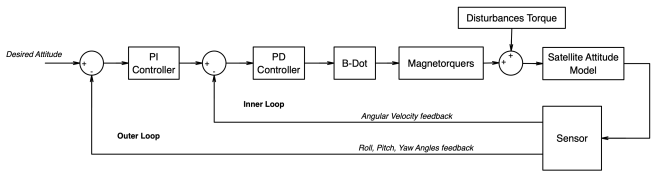

Fig. 2. The structure of a satellite ACS with a cascade PID controller.

the freedom to rotate around its center of mass. In order to describe the satellite's attitude, the Euler angles transform the body frame into an inertial reference frame [10]. The angular rate of the satellite that is represented in the body frame rotates with respect to the inertial reference frame. The dynamic equation of the satellite can be approximated with Euler's moment as follows [11]:

$$\tau = J\dot{\omega} + \omega \times J\omega, \tag{1}$$

where $\tau = (\tau_x, \tau_y, \tau_z)^T$ is the torque vector expressed in the satellite body frame, $\omega = (\omega_x, \omega_y, \omega_z)^T$ is the angular rate, and J is the moment of an inertial matrix of the satellite body frame. Based on magnetic actuation, such as magnetorquer. The Equation (1) then evolves into

$$\tau_{mtq} + \tau_{ext} = J\dot{\omega} + \omega \times J\omega. \tag{2}$$

where τ_{mtq} is the vector of magnetic torques achieved by the magnetorquers and τ_{ext} is the vector of external disturbance torques [12].

The attitude kinematics differential equation when using Euler angles [13] with quaternions can be found in Equation (3) [14], where $q = (q_0, q)$, q_0 is the real part, $q = (q_1, q_2, q_3)$ is the imaginary part, and i, j, and k are unit vectors of the quaternion.

$$\dot{q} = \begin{bmatrix} \dot{q}_0 \\ \dot{q}_1 \\ \dot{q}_2 \\ \dot{q}_3 \end{bmatrix} = \frac{1}{2} \begin{bmatrix} 0 & -\omega_x & -\omega_y & -\omega_z \\ \omega_x & 0 & \omega_z & -\omega_y \\ \omega_y & -\omega_z & 0 & \omega_x \\ \omega_z & \omega_y & -\omega_x & 0 \end{bmatrix} \begin{bmatrix} q_0 \\ q_1 \\ q_2 \\ q_3 \end{bmatrix}. \tag{3}$$

where ω_x, ω_y, and ω_z are the angular velocities of the satellite about each axis.

In order to achieve the aim of reducing the angular rate, the de-tumbling controller is required. The B-dot controller is a control law used to de-tumble satellites. This project chose the B-dot controller because it was concluded to be the best, easiest, and most common controller for de-tumbling satellites [15]. It is written as Equation (4),

$$m_b = \frac{-k_b}{||B||}\dot{B}, \tag{4}$$

where m_b is a vector of the commanded magnetic dipole moment generated by the magnetorquers, k_b is a definite positive gain matrix, and $\dot{B}$ is the opposite sign of the time derivative of the measured magnetic field in the body frame. This can be approximated by $\dot{B} \approx B \times \omega$.

In this project, the de-tumbling and pointing control algorithms will be written in MATLAB to test the satellite magnetic-based ACS, then verified after adding a control strategy in the experimental results section.

B. Satellite Attitude Model and Control System

The closed-loop of satellite magnetic-based ACS includes magnetorquers, attitude sensors, an attitude controller, and a satellite model. In this paper, the cascade PID controller is designed to control the attitude of the satellite model. The structure of the discrete-time PID controller has the form in Equation (5).

$$\begin{aligned} u(k) = u(k-1) \ + \ (K_p + K_i\frac{T}{2} + \frac{K_d}{T})e(k) \ + \\ (-K_p + K_i\frac{T}{2} - \frac{K_d}{T})e(k-1) \ + \ \frac{K_d}{T}e(k-2), \end{aligned} \tag{5}$$

where $e(k) = r(k) - y(k)$ is the system error, K_p is the proportional gain, K_i is the integral gain, K_d is the derivative gain, k is the sampling index, and T is a sampling period.

The cascade PID controller is designed to be applied to this task and includes two control loops: an inner loop with a primary PD controller to control the angular rate and an outer loop with a secondary PI controller to control the Euler angles. A satellite model and the designed cascade PID controller are summarized in the diagram from Figure 2. The PI controller is designed to reduce the error attitude Euler angles (e_{ang}) of the satellite model, and the output of the PI controller provides the reference for the inner loop (r_{vel}), which can be expressed as Equation (6).

$$\begin{aligned} r_{vel}(k) = r_{vel}(k-1) \ + \ (K_{p,ang} + K_{i,ang}\frac{T}{2})e_{ang}(k) \\ + \ (-K_{p,ang} + K_{i,ang}\frac{T}{2})e_{ang}(k-1), \end{aligned} \tag{6}$$

where $e_{ang}(k) = r_{ang}(k) - y_{ang}(k)$ is the Euler angle system error. The PD controller adjusts the angular rate. There is a relationship between angular rate and Euler angles. Any change in the angular rate causes a change in the Euler angles. Therefore, the angular rate is controlled by changing the Euler angles to the desired attitude. The control signal u_{sat} of the satellite magnetic-based ACS with cascade PID controller is calculated using Equation (7).

$$\begin{aligned} u_{sat}(k) = u_{sat}(k-1) \ + \ (K_{p,vel} + \frac{K_{d,vel}}{T})e_{vel}(k) \ + \\ (-K_{p,vel} - \frac{K_{d,vel}}{T})e_{vel}(k-1) \ + \ \frac{K_{d,vel}}{T}e_{vel}(k-2). \end{aligned} \tag{7}$$

where $e_{vel}(k) = r_{vel}(k) - y_{vel}(k)$ is the angular rate system error.

C. Magnetorquer Model

A magnetorquer is one type of actuator for controlling satellite attitude. A magnetic dipole moment $m = (m_x, m_y, m_z)^T$ is generated from the coil part to interact with the earth's magnetic field to generate torque to control the orientation of the satellite, where the current magnitude regulates the strength of the dipole moment. The control torque produced by magnetorquers is given by [15]; $\tau_{mtq} = m \times B$, where $B = (B_x, B_y, B_z)^T$ is the magnetic field in the body frame.

Table 2 shows the typical parameters of three-axis square air-core magnetorquer actuators designed for this task. Figure 3 depicts three orthogonal magnetorquer that must be

TABLE II
MAGNETORQUER PARAMETERS

Parameter	Value
Dimensions [mm]	200 x 200 x 10
Number of turns	250
AWG22 Copper wire diameter [mm]	0.6426
Effective area [m^2]	3.497 x 10^{-2}
Resistance	9.7
Maximum magnetic dipole moment @ 0.92 A [Am^2]	8.19
Mass [g]	637.8

independently controlled on each axis. Each air core magnetorquer's magnetic moment is represented by; $m = i \cdot n \cdot A$.

where i is the current, n is the number of windings in the coil and A is the area enclosed by a turn of the coil's spiral.

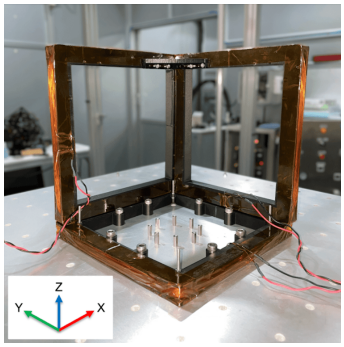

Fig. 3. The three orthogonal magnetorquers.

The percentage difference in the magnetic field intensity given by magnetorquers is verified by comparing the magnetic field intensity between calculating and measuring to confirm the accuracy of magnetorquers. The magnetic field intensity of the magnetorquer m_{mtq} is calculated through Biot-Savart's law in Equation (8),

$$B_{mtq}(z) = \frac{2\mu_0 nia_{sq}^2}{\pi}\left[(a_{sq}^2 + z^2)^{-1}(2a_{sq}^2 + z^2)^{-\frac{1}{2}}\right], \quad (8)$$

where z is the measure point distance on the z-axis 0 to 120 mm each 10 mm for this task, $\mu_0 = 4\pi \times 10^{-7}$ H/m is the magnetic constant, and a_{sq} is the haft length of the square coil, which is 93.5 mm. The Group3 DTM-130 digital teslameter is used in the validation.

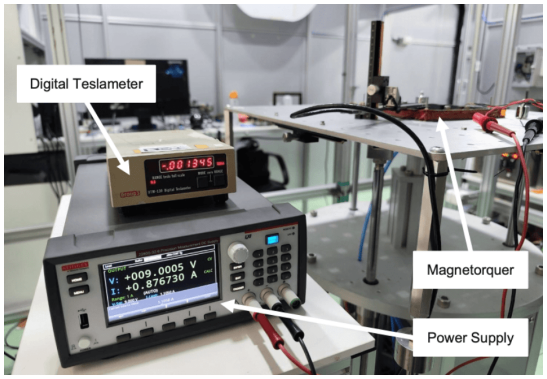

Fig. 4. The magnetic field measurement of the magnetorquer was done using a Group3 DTM-130 digital teslameter and supplied power from 0V to 15V.

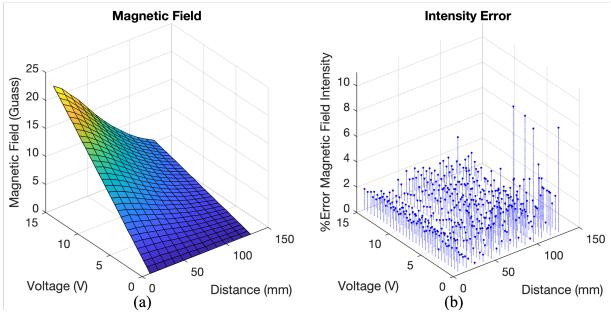

Fig. 5. (a) A 3D surface plot relationship between the measured magnetic field and (b) the magnetic field intensity error of the magnetorquer.

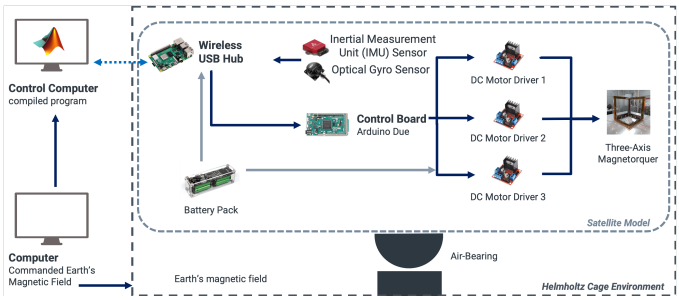

Fig. 6. Block diagram of the HiLs platform.

A power voltage of 0V to 15V is supplied to the magnetorquer at 0.5V to measure the actual magnetic field received (B_{mea}). As shown in Figure 4, the percentage difference of magnetic field intensity (%error) can be defined as follows:

$$\%error = \frac{B_{mtq} - B_{mea}}{B_{mea}} \times 100. \quad (9)$$

The validation result of the magnetorquer model accuracy is described in Figure 5. (a) represents a 3D surface plot relationship between the measured magnetic field from supplied power voltage 0V to 15V and the measuring point distance on the z-axis of the magnetorquer model, and (b) shows the magnetic field intensity error of the magnetorquer. The average percentage difference of magnetic field intensity between calculating and measuring at the measuring point distance on the z-axis of 0 to 120 mm, each 10 mm, is 1.26%. It can be seen that the intensity of the measured magnetic field depends on the measuring point distance. The magnetic field intensity will decrease at a more distant measurement point. The magnetic dipole moment is calculated using Equation (10) below.

$$m_{mea} = \frac{4B_{mea}(z)\pi}{2\mu_0}\left[(a_{sq}^2 + z^2)^1(2a_{sq}^2 + z^2)^{\frac{1}{2}}\right], \quad (10)$$

where m_{mea} is the measured magnetic dipole moment of the magnetorquer and the maximum magnetic moment of the designed magnetorquer at limited current is 0.92. A copper coil, AWG22, is 8.19 Am^2, which is enough to generate torque to detumble the satellite model in the HiLs testing.

D. HiLs Platform

The HiLs platform is used to simulate the de-tumbling phase by creating dynamic motions with an air-bearing platform that enables quasi-frictionless rotational motion to

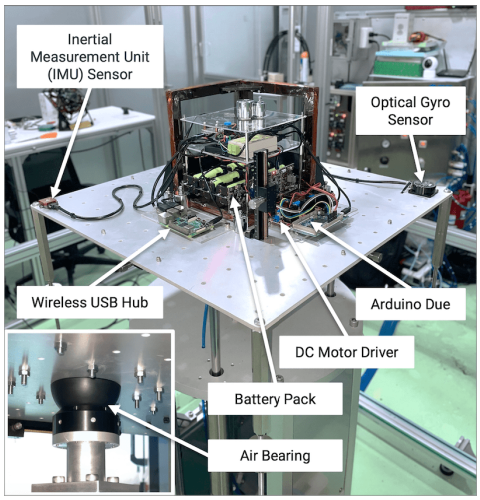

Fig. 7. The components of the HiLs platform.

validate the attitude control algorithm. The HiLs platform is represented in a block diagram in Figure 6.

The control computer obtains attitude data from the sensors as well as the magnetic field command, which is then transmitted to the Helmholtz cage to simulate the EMF. Following that, the control algorithms developed in MATLAB are executed, and the corresponding driving current data is sent through the Raspberry Pi 4, which acts as a wireless USB hub, to the Arduino Due control board. Then the voltage commands from the control board are sent to drive the magnetorquers through DC motor drivers to generate a magnetic field to interact with the EMF from the Helmholtz cage until the satellite model stops tumbling and reaches the desired attitude.

To enable current control on the load, the magnetorquers are powered by three L298N DC motor drivers. These drivers are capable of delivering a maximum current of 2A with a power capacity of 25W. The current control is achieved by utilizing pulse width modulation (PWM) to apply a command voltage to the load. This PWM modulation adjusts the duty cycle of the command, thereby controlling the current flow. Two attitude sensors are used to measure, including the VectorNav VN-100T IMU sensor and the Wit-motion HWT101CT optical gyro sensor, and The battery pack's capacity of 160 Wh is a voltage source for USB hub wireless and DC motor drivers. The components of the HiLs platform are shown in Figure 7.

IV. Experimental Results

In this section, the HiLs testing is used to validate the satellite magnetic-based ACS, and the de-tumbling control in yaw using the B-Dot algorithm with the cascade PID control is designed to investigate the satellite magnetic-based ACS's capability and effectiveness in ground-based testing.

In order to test de-tumbling control of the magnetorquers around the yaw axis, the initial condition for yaw rotational motion was created by accelerating to reach a constant angular rate and produce torque. After that, the satellite magnetic-based ACS starts to de-tumble the satellite model. In this experimental, the constant EMF from Helmholtz cage $\overrightarrow{B}_{emf}$ and the satellite model's initial constant angular rate ω_{int} on air-bearing were set to $\overrightarrow{B}_{emf} = (0.226,\ 0.122,\ 0.453)^T$ G and $\omega_{int} = (0,\ 0,\ 0.0698)^T$ rad/sec, respectively. The B-Dot controller gains of this testing are 100, and the cascade PID positive gains, including $(K_{p,ang}$ and $K_{i,ang})$ of the PI controller and $(K_{p,vel}$ and $K_{d,vel})$ of the PD controller, are tuned by trial and error to find the optimal gains of this satellite model. The simulation parameters and satellite inertial properties for the HiLs testing are indicated in Table 3.

TABLE III
Simulation Parameters for HiLs

Parameter	Value
$\overrightarrow{B}_{emf}$ [G]	$0.226,\ 0.122,\ 0.453$
ω_{ini} [rad/sec]	$0,\ 0,\ 0.0698$
Sampling period (T) [sec]	0.05
B-Dot controller gain (k_b)	$100,\ 100,\ 100$
PI controller gain	$K_{p,ang} = (10.5,\ 10,\ 9)$ $K_{i,ang} = (0.7,\ 0.8,\ 0.9)$
PD controller gain	$K_{p,vel} = (0.14,\ 0.14,\ 0.12)$ $K_{d,vel} = (0.6,\ 0.55,\ 0.6)$
Inertial properties (J) [kgm^2]	$J = (0.5462,\ 0.5442,\ 0.8936)$

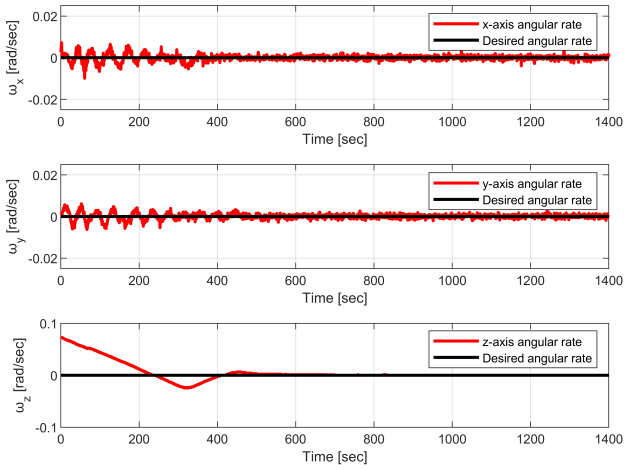

Fig. 8. The angular rate results of the HiLs with the cascade PID controller.

The angular rate results of the control algorithm are shown in Figure 8. The different axes are represented by their own graphs. The angular rate of the x, y, and z axes is settled to the target values (0, 0, 0) rad/sec to complete de-tumbling with 322.26 sec peak time, 33.82% overshoot, and settling time within 568.88 sec at 0.0011 steady state error lower than 2% acceptable.

Figure 9 shows the behavior in time of pointing control in the initial conditions to the desired attitude at Euler angles $(\phi,\ \theta,\ \psi) = (0,\ 0,\ 0)$ deg. From the experimental results, the roll and pitch angles are stabilized within 450 sec, and the yaw angle settles within 892.43 sec at a steady-state error of 3.58, lower than 2% acceptable.

The experimental results of this testing are represented. The B-Dot algorithm with the cascade PID controller de-tumbles the satellite model and points to the desired attitude. The elapsed time to stabilize, reduce the angular rate and orient the satellite model to the desired attitude is 892.43 sec. In contrast, the satellite model on air-bearing keeps rotation in

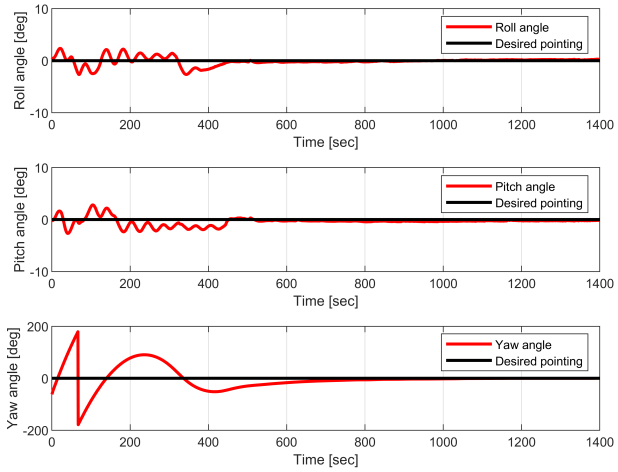

Fig. 9. The Euler angle results of the HiLs with the cascade PID controller.

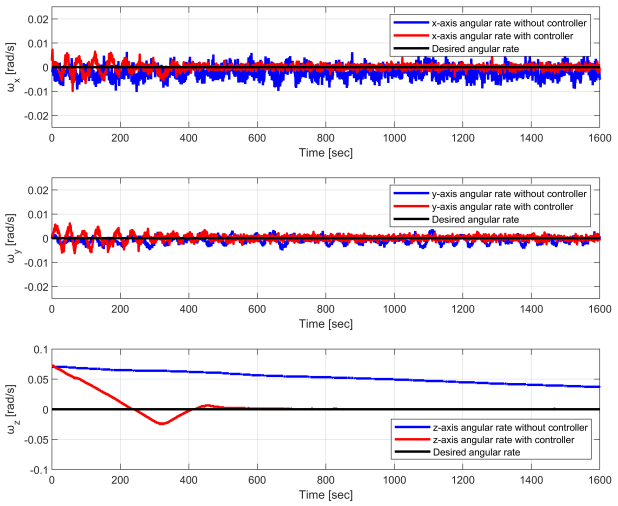

Fig. 10. The angular rate results with and without the control algorithm.

the z-axis without the control algorithm, as shown in Figure 10.

V. Conclusion

The satellite magnetic-based ACS using the three-axis magnetorquer has been developed and tested through the HiLs in the de-tumbling phase, including the Helmholtz cage, which simulates the EMF in orbit, the air-bearing, which enables quasi-frictionless rotational motion, and the on-board computer. Then the control algorithm using a cascaded PID controller is verified. The experimental results provide critical testing capabilities for magnetic-based ACS.

The experimental results are well correlated with the HiLs. The cascade PID controller successfully implemented the de-tumbling and pointing control using a three-axis magnetorquer, compared with the free rotation case without the magnetorquer and controller. In addition, the experimental results show that the three-axis de-tumbling reduces the angular rate of the satellite model below 0.0011 rad/sec at a steady-state error lower than 2% acceptable. At the same time, the pointing control strategy allows reaching the desired attitude with an error below 3.58 deg at steady state and a steady state error lower than 2% acceptable. However, this testing only validates the satellite magnetic-based ACS in the constant EMF. Further applications of the HiLs platform are used to validate the satellite magnetic-based ACS under the EMF simulation by tracking the path of the LEO satellite in SGP4 orbit and verifying the advanced attitude estimation and control strategies validation in modern control approaches such as quadratic regulator controller (LQR) and Model Predictive Control (MPC) to control the nonlinear dynamics system of the satellite model through HiLs on-ground testing platform.

Acknowledgment

Special thanks to the National Research Council of Thailand for their financial support that facilitated the success of our research through the Hub of Talents in Spacecraft Scientific Payload, Grant No. N35E660131, and the Hub of Knowledge in Space Technology and its Application, Grant No. N35E660132. Moreover, we also wish to acknowledge the PBP CMU Electron Linac Laboratory (PCELL) at the Plasma and Beam Physics Research Facility of Chiang Mai University, Thailand, which supports the measuring equipment to validate the magnetic actuator in this experiment.

References

[1] J. N. Pelton and S. Madry, *Handbook of Small Satellites: Technology, Design, Manufacture, Applications, Economics and Regulation*. Springer, 2020.

[2] E. Silani and M. Lovera, "Magnetic spacecraft attitude control: a survey and some new results," *Control engineering practice*, vol. 13, no. 3, pp. 357–371, 2005.

[3] G. Avanzini and F. Giulietti, "Magnetic detumbling of a rigid spacecraft," *Journal of guidance, control, and dynamics*, vol. 35, no. 4, pp. 1326–1334, 2012.

[4] J. Chaisakulsurin, S. Manuthasna, T. Masri, T. Panyalert, K. Palee, P. Prasit, P. Kamsing, and P. Torteeka, "Hardware-in-the-loop simulation testbed for three-axis earth's magnetic field generation based on 2.4-meter square helmholtz coils," in *2023 IEEE/ION Position, Location and Navigation Symposium (PLANS)*, 2023, pp. 829–834.

[5] R. C. da Silva, I. S. K. Ishioka, C. Cappelletti, S. Battistini, and R. A. Borges, "Helmholtz cage design and validation for nanosatellites hwil testing," *IEEE Transactions on Aerospace and Electronic Systems*, vol. 55, no. 6, pp. 3050–3061, 2019.

[6] S. Corpino and F. Stesina, "Verification of a cubesat via hardware-in-the-loop simulation," *IEEE Transactions on Aerospace and Electronic Systems*, vol. 50, no. 4, pp. 2807–2818, 2014.

[7] L. Li, J. Yang, X. Shi, and H. Liu, "Robust attitude control for flexible satellite during orbit maneuver," in *Proceedings of 2014 IEEE Chinese Guidance, Navigation and Control Conference*. IEEE, 2014, pp. 2531–2536.

[8] X. Yi and A. Anvar, "Small-satellite magnetorquer attitude control system modelling and simulation," 2013.

[9] G. Cervettini, S. Pastorelli, H. Park, D. Y. Lee, and M. Romano, "Development and experimentation of a cubesat magnetic attitude control system testbed," *IEEE Transactions on Aerospace and Electronic Systems*, vol. 57, no. 2, pp. 1345–1350, 2020.

[10] H. D. Curtis, *Orbital mechanics for engineering students*. Butterworth-Heinemann, 2013.

[11] M. C. Mahdi, *Attitude stabilization for CubeSat: concepts and technology*. Cambridge Scholars Publishing, 2018.

[12] J. R. Wertz, *Spacecraft attitude determination and control*. Springer Science & Business Media, 2012, vol. 73.

[13] H. Schaub and J. L. Junkins, *Analytical mechanics of space systems*. Aiaa, 2003.

[14] Y. Yang, *Spacecraft modeling, attitude determination, and control: quaternion-based approach*. CRC Press, 2019.

[15] F. L. Markley and J. L. Crassidis, *Fundamentals of spacecraft attitude determination and control*. Springer, 2014, vol. 1286.